IEEE Access
Multidisciplinary ⋮ Rapid Review ⋮ Open Access Journal

Received November 3, 2020, accepted November 14, 2020, date of publication November 24, 2020,
date of current version December 9, 2020.

Digital Object Identifier 10.1109/ACCESS.2020.3040099

Review of Local Network Impedance Estimation Techniques

MATHIEU KERVYN DE MEERENDRE[1], (Student Member, IEEE), EDUARDO PRIETO-ARAUJO[2], (Member, IEEE), KHALED H. AHMED[1], (Senior Member, IEEE), ORIOL GOMIS-BELLMUNT[2], (Senior Member, IEEE), LIE XU[1], (Senior Member, IEEE), AND AGUSTÍ EGEA-ÀLVAREZ[1], (Member, IEEE)

[1]Electronic and Electrical Engineering Department, University of Strathclyde, Glasgow G1 1XW, U.K.
[2]Electrical Engineering Department, Centre d'Innovació Tecnològica en Convertidors Estàtics i Accionaments (CITCEA-UPC), Universitat Politècnica de Catalunya, 08028 Barcelona, Spain

Corresponding author: Mathieu Kervyn de Meerendre (mathieu.kervyn@strath.ac.uk)

This work was supported in part by the Engineering and Physical Sciences Research Council, National Productivity Investment Fund, under Grant EP/R512205/1.

ABSTRACT As a result of increasing variability of network impedance, interest in impedance estimation techniques is growing. This review contextualises local impedance estimation techniques by providing a historical prospective on the uses of these techniques, from the early implementations designed to monitor power quality to the latest techniques integrated into converters designed to update the controller with the most recent network information. This is followed by clear and consolidated descriptions, a complete classification and comparison tables of local estimation techniques intended to assist engineers and researchers choose an estimation technique that is suitable to their application. The discussed techniques are then ranked for a range of application priorities such as accuracy, least disruptive to the network, most suitable for wide frequency spectrum estimations and rapidity of estimation. Practical applications of impedance estimation are discussed, such as network characterisation, anti-islanding detection, filter resonance avoidance and controller tuning. To conclude the review, future trends are identified.

INDEX TERMS Frequency sweep, impedance estimation, impedance identification, impulse-response, Kalman filter, observer, P/Q variation, phasor measurement units, pseudo random binary sequence, review.

NOMENCLATURE

For the power system and most estimation techniques:

- C_f Filter capacitance.
- E Stiff grid voltage magnitude.
- I_c Current at generator magnitude.
- I_n Current at grid magnitude.
- L_c Inductive element of filter.
- L_n Inductive element of grid impedance.
- R_c Filter resistance.
- R_n Grid resistance.
- U PCC voltage magnitude.
- V Converter or generator output voltage magnitude.
- X_n Grid reactance.
- β Angle of grid voltage.
- Γ Quality threshold.
- θ Angle of PCC voltage.
- ω Frequency of the impedance undergoing analysis.

For notation used in equations for recursive least squares:

- $\boldsymbol{A}$ Matrix of grid currents and ones.
- $\boldsymbol{Q}$ Error between $\boldsymbol{X}$ and $\hat{\boldsymbol{X}}$.
- $\boldsymbol{X}$ Inductance and grid voltage vector.
- $\hat{\boldsymbol{X}}$ Estimate of $\boldsymbol{X}$.
- $\boldsymbol{Y}$ Output vector.

For notation used in equations for Kalman Filter:

- $\boldsymbol{A}$ State matrix.
- $\boldsymbol{B}$ Input matrix.
- $\boldsymbol{C}$ Output matrix.
- $\boldsymbol{I}$ Identity matrix.
- k Iteration number.
- $\boldsymbol{K}$ Kalman Gain.

The associate editor coordinating the review of this manuscript and approving it for publication was Sze Sing Lee.

$\boldsymbol{M}$ Expected white noise of the estimation process.
$\boldsymbol{N}$ Expected measurement noise.
$\boldsymbol{P}$ Error covariance of states.
$\boldsymbol{u}$ Input vector.
$\boldsymbol{V}$ Predicted estimation error.
$\boldsymbol{x}$ State vector.
$\hat{\boldsymbol{x}}$ State estimate vector.
$\boldsymbol{y}$ Output vector.
$\hat{\boldsymbol{y}}$ Output estimate vector.

I. INTRODUCTION

Early impedance estimation literature focused on harmonic content due to power quality concerns [1], [2]. A guide for network harmonic impedance assessment was written by a CIGRE/CIRED Working Group CC02 [3]. The main motivation behind the early literature and the CIGRE/CIRED report was to improve the understanding of the harmonic current caused by power equipment in the network. The identification of resonant frequencies through wide frequency spectrum impedance estimation allowed for the design of harmonic filters and capacitor banks, reducing the resonances and improving power quality [4]. Some of the proposed techniques utilised harmonic excitation (frequency sweeping) with dedicated hardware [1], [5]. Others generated an impulse by close-trip operations of a shunt capacitor bank, causing a large inrush of current and rich spectral excitation [2], [3]. Alternatively, [6]–[8] utilise thyristor switches, creating a short circuit and subsequent large current pulse injection, with the intention of monitoring in real-time the evolution of network impedance. [9], [10] exploit the resonances of LCL-filters to excite the system.

With the advancement of microcontroller computational capabilities, online impedance estimators became increasingly common in the literature. Anti-islanding is a common motivation for impedance estimation literature [11]–[16], with the draft European standard EN50330-1 (or equivalent German standard VDE0126) usually cited as a justification. For completeness, EN50330-1 is now cancelled, and the current standard regarding islanding prevention is EN62116, *Utility-interconnected photo-voltaic inverters – Test procedure of islanding prevention measures* [17]. The estimation techniques employed in [12]–[14] are based on the injection of a nonharmonic current, followed by fast Fourier transform (FFT) of the nonharmonic frequency current and voltage response. [15], [18] collected information about the system by varying the outer loop active power (P) and reactive power (Q) references.

Recent literature is particularly interested in online controller tuning for improved stability [19]–[25]. Many of these articles are driven by increased network impedance variability and resulting voltage stability issues [26], consequently increasing the importance of appropriate control tuning [27]. Such impedance variability is a direct result of changes in how the network is used (renewable energy sources are being connected in geographically remote locations) [28]–[32] and the increase in converters connecting to the network [33]–[35], both of which are affecting the local network impedance from a generator's prospective (renewable or otherwise) and strength of the network as a whole. For completeness, there is also an alternative approach to online controller tuning, and that is to use impedance agnostic control [23], [36]–[42]. However, these techniques may require stability studies as part of the commissioning, studies which could be based on the estimation techniques discussed in this article.

Other authors are motivated by LCL-filter resonances, a phenomenon which is difficult to mitigate in variable impedance networks [43]–[47]. It is demonstrated in [48] that network impedance estimation could help avoid filter resonance issues by retuning the current controller appropriately. [49] also utilises impedance estimations to improve stability of an LCL-filter interfaced converter by adapting the phase-locked loop (PLL) tuning accordingly.

The focus of this review is on local techniques only – network-wide techniques are not considered in this article. While there exists literature with categorisations of local impedance estimation techniques [3], [52], [53], they are either dated, incomplete or too brief. The aim of this article is to consolidate, organise and analyse all the published techniques and supporting documentation more thoroughly, consistently and clearly than the existing literature in order to assist engineers and researchers determine the most suitable estimation technique for their application. This article is up-to-date with the most recent literature.

This article is organised as follows. Section II provides the reader with an overview of the classification system. Passive and active and quasi-passive estimation techniques are described in Sections III, IV and V, respectively. This is followed by a comparison table (Section VI), ranking of the techniques based on implementation objectives (Section VII), further discussion on applications of impedance estimation (Section VIII), and finally future trends (Section IX).

II. CLASSIFICATION OF LOCAL IMPEDANCE ESTIMATION TECHNIQUES

A high level classification of the estimation techniques is presented in Fig. 1. The specific section numbers are included to describe the structure of the article. For a consolidated list of the references, refer to Table 2 in Section VI.

Estimation techniques can be subdivided into active, passive or quasi-passive techniques, depending on whether the perturbation is intentionally and periodically introduced, whether it must occur naturally in the grid, or whether an observer is used to trigger an active estimation technique.

As many discussed techniques are implemented in converters, Fig. 2 displays the reference system diagram, where $\overline{V}$ is the converter voltage, $\overline{I_c}$ is the converter current, R_c, L_c and C_f are the resistance, inductance and capacitance of the converter filter, $\overline{U}$ is the PCC voltage, R_n and L_n are the grid resistance and inductance, and $\overline{E}$ is the grid voltage. The various techniques view the network impedance as an aggregated impedance, which is either assumed linear

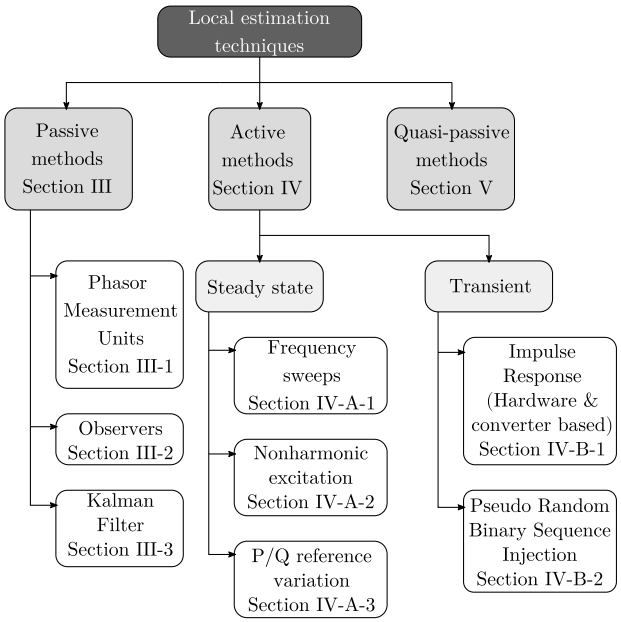

FIGURE 1. Classification of local impedance estimation techniques and relevant section.

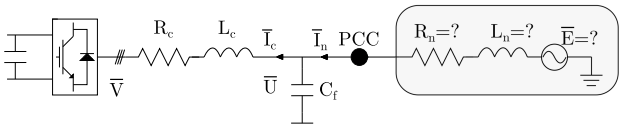

FIGURE 2. Converter connected to PCC, with unknown Thévenin equivalent impedance and equivalent grid voltage marked in the grey box.

and represented by its Thévenin equivalent (R_n and L_n are constant), or considered to be nonlinear ($R_n(\omega)$ and $L_n(\omega)$ are a function of frequency). The bar above the currents and voltages is used to describe a rectangular quantity, with a real and imaginary part. Sometimes these quantities are represented in polar form, in which case an arrow is used. While these quantities are interchangable, it is decided to differentiate between them in order to clarify which representation is used in the appropriate descriptions.

III. PASSIVE TECHNIQUES

Passive techniques utilise existing transients, caused by sufficiently large grid events, to undertake impedance estimations. Passive techniques can be loosely categorised as local PMU derived observers, PCC observers and Kalman Filters.

1) LOCAL PMU DERIVED OBSERVERS

PMUs are used to produce synchrophasor measurements – fundamental frequency voltage and current measurements that are time synchronised [54]. Normally, synchophasors are communicated to a central computer, and this information can be used to undertake state estimation, fault detection/location and wide area monitoring, including protection [55]–[57]. While the use of synchrophasors from multiple PMUs can be used to measure line impedance [51], [58], [59], the focus of this article is on the local techniques which utilise local measurements only. A single PMU, benefiting from the accurate time stamping of phasors, can be used to estimate the Thévenin equivalent properties of the network. The high level procedure is summarised in Fig. 3, where the adaptive technique is based on [60], the recursive least squares (RLS) solver is derived from [61]–[64], and the algebraic technique is derived from [24], [65].

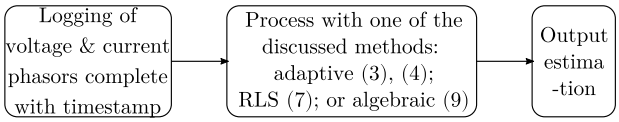

FIGURE 3. Flow chart typical of most local PMU derived observers.

Firstly, regarding the adaptive solver [60], the PCC voltage phasor $\overrightarrow{U}$ can be described as:

$$\overrightarrow{U} = \overrightarrow{E} - \overline{Z}_n \overrightarrow{I_n} \tag{1}$$

where $\overrightarrow{U}$ is the PCC voltage phasor ($\overrightarrow{U} = U\angle\theta$), $\overrightarrow{E}$ is the equivalent grid voltage phasor ($\overrightarrow{E} = E\angle\beta$), $\overrightarrow{I_n}$ is the grid current phasor ($\overrightarrow{I_n} = I_n\angle 0°$), and $\overline{Z}_n$ is the grid impedance ($\overline{Z}_n = R_n + jX_n$). The arrow notation is used to describe phasors, whereas the bar notation is used to describe complex quantities. The phasor relation of $\overrightarrow{U}$, $\overrightarrow{E}$ and $\overrightarrow{I_n}$ is graphically represented in the Fig. 4 phasor diagram.

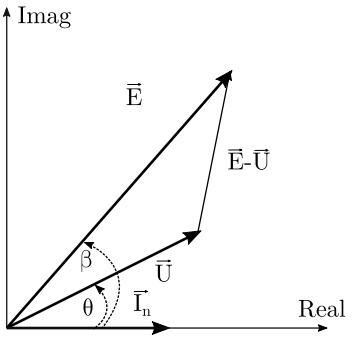

FIGURE 4. Phasor diagrams for local PMU-based estimation techniques.

Given that $\overline{Z}_n = R_n + jX_n$, (1) can be rearranged and separated into real and imaginary components, as follows:

$$E\cos(\beta) = R_n I_n + U\cos(\theta) \tag{2}$$

$$E\sin(\beta) = X_n I_n + U\sin(\theta) \tag{3}$$

In the two above equations, there are four unknowns: E, β, R_n and X_n. However, if the network is known to be much more inductive than resistive ($X_n \gg R_n$), then it is acceptable to assume $R_n = 0$ [60]. This assumption allows the decoupling of X_n from $\overrightarrow{E}$ by rearranging (2):

$$\beta = \cos^{-1}\left(\frac{U\cos(\theta)}{E}\right) \tag{4}$$

In [60], an initial E estimate is made by taking the mean value of the expected voltage region, and updating for a new value

with every consecutive timestep using (3) and (4). Every updated value of E corresponds to a unique value of X_n. The direction of the error for E is dependent on the variations of the load impedance (analogous to the converter output impedance which includes both the filter and the converter) called Z_l. When X_n and Z_l vary in the same direction, estimates of E reduce; otherwise E increases.

Alternatively to the adaptive solver is the RLS solver [61]–[64]. The RLS solver allows an under-determined system to generate a unique set of estimations by allowing the use of many measurement points without making the equations over-determined. RLS is usually undertaken using rectangular notation instead of phasor notation. Using the same notation as Fig. 2, the implementation is as follows:

$$\boldsymbol{Y} = \boldsymbol{A}\hat{\boldsymbol{X}} - \boldsymbol{Q} \tag{5}$$

Expanded in full matrix form

$$\begin{bmatrix} \overline{U}_1 \\ \overline{U}_2 \\ \vdots \\ \overline{U}_k \end{bmatrix} = \begin{bmatrix} \overline{I_{n1}} & 1 \\ \overline{I_{n2}} & 1 \\ \vdots & \vdots \\ \overline{I_{nk}} & 1 \end{bmatrix} \cdot \begin{bmatrix} \hat{\overline{Z}}_n \\ \hat{\overline{E}} \end{bmatrix} - \begin{bmatrix} q_1 \\ q_2 \\ \vdots \\ q_k \end{bmatrix} \tag{6}$$

where $\hat{\boldsymbol{X}}$ is the estimate of $\boldsymbol{X}$ and $\boldsymbol{Q}$ is the error between $\boldsymbol{X}$ and $\hat{\boldsymbol{X}}$. The use of the bar for voltages and current denote rectangular notation, where $\overline{U} = U_{real} + jU_{imag}$, $\overline{E} = E_{real} + jE_{imag}$, and $\overline{I_n} = I_{real} + jI_{imag}$. The RLS technique requires some manipulation [66] which results in (7). This form allows a simple closed-form solution which minimises the error.

$$\hat{\boldsymbol{X}} = (\boldsymbol{A}^T\boldsymbol{A})^{-1}(\boldsymbol{A}^T\boldsymbol{Y}) \tag{7}$$

To conclude the PMU derived observers is the algebraic solvers, described in [24], [65]. In this instance, only two measurement sets are used and solved algebraically, resulting in the following equation. The initial measurement set has the subscript 0, and the following measurement set has the subscript 1.

$$\overline{Z_n} = \frac{\overline{U_1} - \overline{U_0}}{\overline{I_{n1}} - \overline{I_{n0}}} \tag{8}$$

Both above mentioned articles [24], [65] proceed to enhancing the equation, compensating for measurement drift caused by the deviation from fundamental frequency experienced by the signals, as follows:

$$\overline{Z_n} = \frac{\overline{U_1}e^{j\Delta\theta} - \overline{U_0}}{\overline{I_{n1}}e^{j\Delta\theta} - \overline{I_{n0}}} \tag{9}$$

where $\Delta\theta$ is the shift in phase due to the deviation from fundamental frequency.

2) PCC OBSERVERS

This subcategory is relevant to devices with measurement capabilities that do not utilise GPS synchronisation. This is the case for most converters and buses with current and voltage sensors. Observers generally follows the flow chart depicted in Fig. 5 of recognising a grid event, storing the information, and mathematically extracting an impedance estimation, normally in the frequency domain.

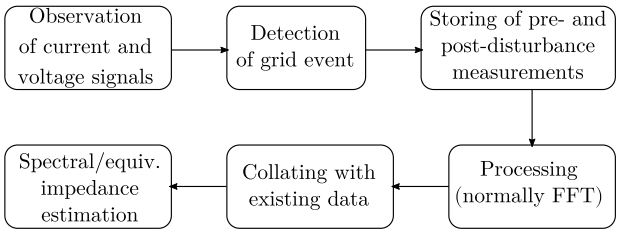

FIGURE 5. Flow chart typical of most observers.

Reference [67] identifies that a sufficiently large grid event has occurred when a 3% change in RMS voltage is registered. The transients caused by such an event can provide information about the system across a wide range of frequencies. Triggered by the transient, the estimation procedure requires the storage of voltage and current measurements for five fundamental periods immediately before and after the event is detected. FFT is then used to convert pre- and post-disturbance voltage and current from the time domain to the frequency domain up to the 50th harmonic, and (10) is used to estimate the impedance, where ω represents the frequency being analysed.

$$\overline{Z_n}(\omega) = \frac{\overline{U}(\omega)_{pre} - \overline{U}(\omega)_{post}}{\overline{I_n}(\omega)_{pre} - \overline{I_n}(\omega)_{post}} = \frac{\Delta\overline{U}(\omega)}{\Delta\overline{I_n}(\omega)} \tag{10}$$

Notice that (10) is similar to (8), with the difference being that (8) is valid for the fundamental frequency impedance only (the Thévenin equivalent), whereas (10) can determine the impedance at a range of frequencies, subject to the FFT implementation.

With the observer implementation described in [67], good estimations require data accumulated by 70 grid events over 15 days – the accuracy of the estimates are not explicitly stated, but this is clear in the article figures. In [68], the same authors presented the same data with the addition of the reference impedance value.

If the impedance estimator is part of a converter controller, the noise induced naturally by the switching of the converter can be used as the basis of disturbances. This is the case in [69] where the switching frequency of 10 kHz introduces voltage and current harmonics into the system. Assuming there is no pre-existing high frequency harmonics in the grid voltage it is demonstrated that results can be obtained within 20 ms. [19] uses a similar process and assumptions, but with more focus on the timing of the samples relative to the space vector pulse width modulation (SV-PWM) switching. An estimation time of 50 ms is achieved. Another article, [70], also utilises PWM induced noise but this time uses the Recursive Least Squares technique as a means of mathematically extracting the impedance information. With a switching frequency of 2.8 kHz, the impedance estimation time is 1.2 s.

An alternative implementation of the observer monitors the variations in active power. A sufficiently large

disturbance within the system, such as a step change in network impedance, will excite the system and cause the active power injection to vary [71]. In [71], FFT is used to extract the Thévenin equivalent impedance when a disturbance is detected using (10). This technique can be classified as passive because the change in power set-point is not undertaken specifically to disturb the system.

3) KALMAN FILTER

Some researchers have recently suggested using nonlinear variations of the Kalman Filter in order to estimate the impedance. Whilst this technique is a type of observer, the computation and implementation is very different to the above mentioned observers – therefore the Kalman Filter is considered separately. The Kalman Filter flow chart is presented in Fig. 6 [72]. It begins with the initialization, and then continually loops around as long as the Kalman Filter continues to receive new system measurements.

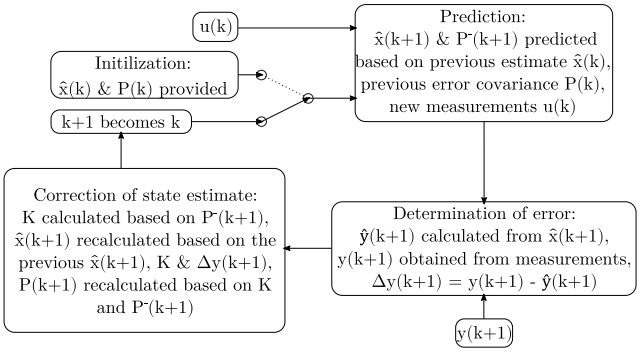

FIGURE 6. Flow chart typical of the extended Kalman Filters.

The Kalman Filter works in roughly three main steps:

The first is the *prediction* step which involves estimating the system states $\hat{\boldsymbol{x}}$ and the error covariance of the states $\boldsymbol{P}^{-}$, as per (11) (12).

$$\hat{\boldsymbol{x}}(k+1|k) = \boldsymbol{A}\hat{\boldsymbol{x}}(k) + \boldsymbol{B}\boldsymbol{u}(k) \tag{11}$$

$$\boldsymbol{P}^{-}(k+1) = \boldsymbol{A}\boldsymbol{P}(k)\boldsymbol{A}^{T} + \boldsymbol{V}\boldsymbol{M}\boldsymbol{V}^{T} \tag{12}$$

where $\boldsymbol{A}$ is the state matrix, $\boldsymbol{B}$ is the input matrix, $\boldsymbol{V}$ is the predicted estimation error and $\boldsymbol{M}$ is the expected white noise of the estimation process.

The second step is to use the state estimations to determine the corresponding outputs $\hat{\boldsymbol{y}}$ (14), and *determine the error* by comparing the measured and estimated output values (14). $\boldsymbol{C}$ is the output matrix.

$$\hat{\boldsymbol{y}}(k+1) = \boldsymbol{C}\hat{\boldsymbol{x}}(k+1|k) \tag{13}$$

$$\boldsymbol{\Delta y}(k+1) = \boldsymbol{y}(k+1) - \hat{\boldsymbol{y}}(k+1) \tag{14}$$

The final step is to *correct the state estimate*. This is done by calculating the new Kalman Gain from the prediction error covariance and the expected measurement noise ($\boldsymbol{N}$) (15), and using the Kalman Gain to undertake a final state estimation (16). The prediction covariance is also subsequently updated (17).

$$\boldsymbol{K}(k+1) = \boldsymbol{P}^{-}(k+1)\boldsymbol{C}^{T}\left(\boldsymbol{C}\boldsymbol{P}^{-}(k+1)\boldsymbol{C}^{T} + \boldsymbol{N}(k+1)\right)^{-1} \tag{15}$$

$$\hat{\boldsymbol{x}}(k+1|k+1) = \hat{\boldsymbol{x}}(k+1|k) + \boldsymbol{K}(k+1)\boldsymbol{\Delta y}(k+1) \tag{16}$$

$$\boldsymbol{P}(k+1) = (\boldsymbol{I} - \boldsymbol{K}(k+1)\boldsymbol{C})\boldsymbol{P}^{-}(k+1) \tag{17}$$

The "extended" Kalman Filter (EKF) is an augmentation of the Kalman Filter intended for nonlinear systems. The EKF is implemented in [73], [74] where a Jacobian matrix is used instead of the state matrix to account for the nonlinearities, demonstrating good results for the assumed Thévenin equivalent system. The authors of [73] do concede, however, that system tuning is complex, requiring EKF optimisation through trial and error for the various grid conditions and operating points.

IV. ACTIVE TECHNIQUES

Active techniques, unlike passive techniques, do not rely on existing grid events. Instead, these techniques intentionally introduce a controlled perturbation or change in operating point, increasing the information available about the network. Active techniques can be further subcategorised into steady state and transient techniques.

A. STEADY STATE

Steady state techniques require the network response to a perturbation to settle prior to the collection of any measurement. All steady state techniques assume stationary network conditions for the duration of the testing.

1) FREQUENCY SWEEPS

Frequency sweeps remain the most common grid characterisation technique, normally employed for network studies at a PCC [1]. Typical implementation is demonstrated in the Fig. 7.

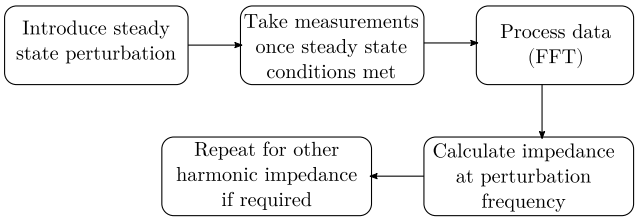

FIGURE 7. Flow chart for frequency sweeping.

Frequency sweeps are usually undertaken by attaching specialised hardware at the point of interest [52], injecting small steady state sinusoidal perturbations at a wide range of frequencies, and employing Fourier analysis to calculate the network impedance in the frequency domain, as per (18) where ω represents the perturbation frequency [5], [75]. Note that the perturbation frequency must be different to the fundamental frequency. Assuming that the network is stationary for the duration of the test, the wide spectrum impedance

analysis can provide detailed grid characterisation complete with nonlinearities (such as resonances) at the cost of lengthy testing duration [3]. Frequency sweeping can be undertaken with specialised equipment installed temporarily in a node of the system or via standard grid-connected power converters. [76] focuses on line impedance estimation.

$$\overline{Z_n}(\omega) = \frac{\overline{U}(\omega)}{\overline{I_n}(\omega)} \tag{18}$$

This type of analysis has been further developed, with [52] using inexpensive hardware to estimate impedance from 20 Hz to 24 kHz, [77] using high resolution equipment to estimate the the impedance from 2 to 150 kHz, and [78] undertaking frequency sweeps of multiple frequencies simultaneously, increasing the data captured with each sweep. Frequency sweeps are not used only in utility grids but also in contained systems, such as on aircraft and ships [79], [80].

Wide spectrum frequency sweeps are occasionally implemented in converters as a means of validating the laboratory results of alternative impedance estimators – such as [81] (impulse-response) and [82] (pseudo random binary sequence injection).

2) NONHARMONIC EXCITATION

A number of publications choose to assume linear impedance and only excite a single noncharacteristic frequency. This is known as nonharmonic excitation. For example, [11], [13], [14] inject a noncharacteristic harmonic current of 75 Hz periodically. The settled values of current and voltage are recorded and converted into the frequency domain with Fourier transform analysis (or wavelet transform as per [11]). The voltage and current values at 75 Hz are extracted and the impedance is calculated with $\overline{Z_n}(\omega_h) = R_n + j\omega_h L_n$ (where ω_h is the nonharmonic frequency). It is assumed that the impedance at 75 Hz and 50 Hz is the same. [12] provides a very similar methodology, except that the period in between disturbances is 5 seconds. [83], [84] excites at 400 and 600 Hz, except that in [84] voltage is excited instead of the current. Interestingly, [85] excites a frequency of 10 Hz. Of the implementations discussed in this section, only [83]–[85] calculated both resistance and reactance as separate parameters – all other implementations only calculated the impedance magnitude. Nonharmonic perturbations can be injected in the dq-frame as per Fig. 8.

More recently, some researchers have explored using the Wavelet Transform (WT) as an alternative to FFT [11], [86]. The perturbations are the same as previously explained, with nonharmonic frequencies of 75 and 630 Hz utilised in these articles, and with both inductance and resistance estimated. The WT is explained in more detail at the end of Section IV-B1 as it is generally more appropriate to transient methods.

As an aside, the WT is not limited to impulse-response. utilises the WT combined with a steady state nonharmonic current injection.

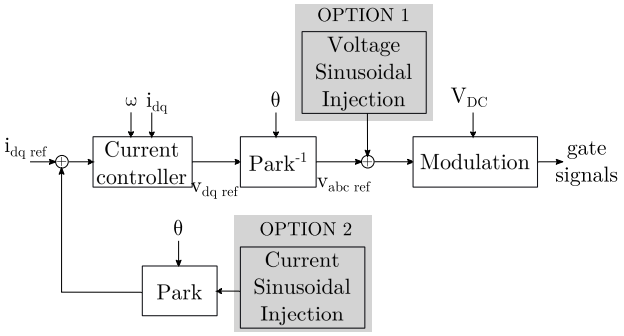

FIGURE 8. Examples of current and voltage sinusoidal injection within vector control.

3) P/Q REFERENCE VARIATION

The final steady state technique is the P/Q reference variation technique. In this technique, the active power and reactive power references are intentionally varied in order to allow the detection of both the resistive and inductive parts of the network Thévenin equivalent impedance [87]. With variations in outer loop references, the P/Q reference variation technique causes a very small amount of noise and disruption in the network [87]. This is described in Fig. 9.

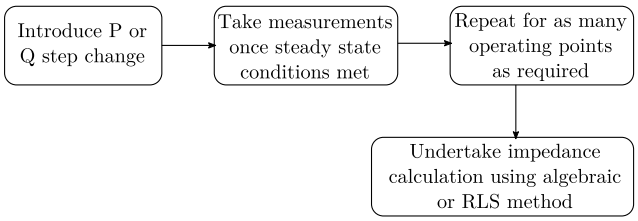

FIGURE 9. Flow chart of P/Q reference variation.

The techniques described in [25], [53], [87], [88] require two sets of measurements, where P and Q deviations can be either positive or negative. The impedance is subsequently calculated algebraically as per (19) and (20), or similar. The Park transformation values for PCC voltage and grid current are used, such that $\overline{U} = U_q - jU_d$ and $\overline{I_n} = I_{nq} - jI_{nd}$. Subscripts 1 and 2 represent the two sets of measurements.

$$R_n = \frac{(U_{q1} - U_{q2})(I_{nq1} - I_{nq2}) + (U_{d1} - U_{d2})(I_{nd1} - I_{nd2})}{(I_{nq1} - I_{nq2})^2 + (I_{nd1} - I_{nd2})^2} \tag{19}$$

$$L_n = \frac{1}{\omega_0} \frac{(U_{d1} - U_{d2})(I_{nq1} - I_{nq2}) - (U_{q1} - U_{q2})(I_{nd1} - I_{nd2})}{(I_{nq1} - I_{nq2})^2 + (I_{nd1} - I_{nd2})^2} \tag{20}$$

The P/Q variation technique is further expanded in [15], [89] to use a RLS solver. The RLS solver is already described earlier in (5), (6) and (7) and the analysis techniques are the same. However, when implemented in a converter, the active and reactive power can be controlled to ensure variability in operating points. This is demonstrated in Fig. 10, where three different measurement sets are used.

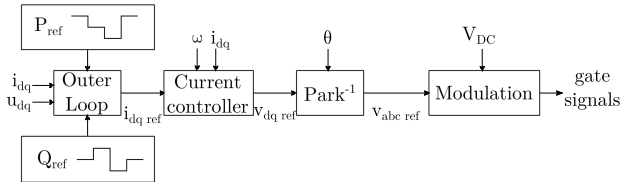

FIGURE 10. PQ variation with 3 different measurement points.

Recent publications have seen principles of the P/Q variation technique applied to relatively new concepts. [90] has adapted the P/Q variation technique to grid forming converter control, demonstrated to work in both voltage and power control cases; and [91] has implemented the method to a system with no direct voltage measurements and only active power variation.

B. TRANSIENT TECHNIQUES

Unlike active techniques, transient techniques utilise the immediate transient response to a perturbation in order to extract information about the network. The most common form of transient technique is the impulse-response technique, but a number of articles also use the pseudo random binary sequence injection technique.

Irrespective of the nature of the perturbation, the impedance calculation is as follows – taking into account both the pre-disturbance and post-disturbance measurements [8], [92]. Notice that this is the same equation as (10) – the calculation is the same, the difference is simply in whether the disturbance is detected or intentionally injected.

$$\overline{Z_n}(\omega) = \frac{\Delta\overline{U}(\omega)}{\Delta\overline{I_n}(\omega)} \tag{21}$$

1) IMPULSE-RESPONSE

The impulse-response technique involves injecting a current or voltage perturbation pulse into the network in order to obtain a response for a wide range of frequencies [93], with the flow chart presented in Fig. 11. Given the short duration of the impulse, the size of the frequency spectrum of interest and the possibility of high signal to noise ratio (SNR), the impulse must be large [3], [92]. This allows for full spectral excitation in a very short period of time, making this technique particularly attractive in highly variable networks [7]. As such, additional hardware is often used to generate the impulse (such as the 5 pu of current injected in [8]). The use

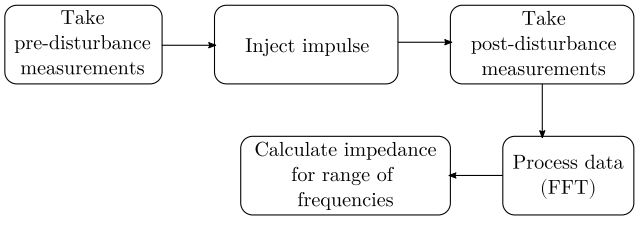

FIGURE 11. Flow chart for the impulse technique.

of additional hardware also allows for the disturbance to be injected directly in the PCC of interest, making the estimation of both the converter output impedance and grid impedance possible. Examples of hardware for impulse generation are shunt capacitor banks [2], [3], [92], the use of thyristor switches to create a short circuit [8], [94], or even switching the DC link voltage across an L filter inductor [93]. [81] use a dedicated power converter for increased control over the disturbance, as does [95], where the injected rectangular impulse is designed to extract impedance information at frequencies 2 kHz to 150 kHz.

Not all articles using the impulse-response technique rely on additional hardware. Some have implemented the impulse-response technique directly into a converter. Unlike the aforementioned techniques that use dedicated impulse generating hardware, converter based injections are limited by the rating of the converter. Motivation for the impedance estimation vary from the identification of stability margins [96] to online PLL bandwidth adaptive control [97]. Due to the wide number of varying features described in impulse-response literature, Table 1 has been produced to simplify the comparison process.

Table 1 identifies whether the impulse is a voltage or a current; the type of filter used (L or LCL-filter); the type of grid that is being assessed (sometimes the grid is assumed to be a simple inductor with no resistance, but other times it is more complex with parallel branches and multiple resonances); the properties of the injection, including the per unit value if it is provided or calculable; the injection width in micro or milliseconds, the number of measurements taken, the frequency range processed by the FFT, and a note on how the technique is validated. Note that only [49], [81], [96], [98] are online, with complete microcontroller integration of the estimation technique.

From Table 1, it can be deduced that even converter-implemented impulse-response techniques inject a significant disturbance into the network, with the majority of implementations injecting at least 0.5 pu of base current or voltage. However, this allows for a very short measurement period and an impedance estimation covering a large range of frequencies (almost all variations measure up to 2 kHz). In general, measurement periods are even shorter if the impulse is larger (i.e. 1.5 pu impulse). The types of grids varies greatly, from simple inductors to complex networks with parallel capacitors, therefore introducing resonant behaviour and replicating certain grid behaviours.

With regards to the converter controller, there are two main implementations of the converter induced impulse. Either it is injected as a current in the d-component of the current reference [96], or as a voltage in the q-component of the voltage reference during the zero crossing [98]. These are represented graphically in Fig. 12.

As an alternative to the FFT, the impulse-response technique could utilise the Wavelet Transform (WT) as a means of analysing measurement results, as per [100]. The difference between FFT and WT is that FFT compares a given signal

TABLE 1. Various implementations of the converter injected impulse-response technique.

Ref	Dist. type	Filter	Type of grid	Injection properties	Injection width	Measurements	Target frequency range	How is it validated?
[81]	V	L	Circuit 1: L only Circuit 2: L parallel with C	Triangular	500 μs	8 transient cycles and 8 steady state cycles	< 1 kHz	Freq sweeps
[99]	V	L	Circuit 1: RL Circuit 2: RL parallel with RC Circuit 3: Multiple resonances	Stepped injection with a maximum amplitude of $\sim$ 0.5 pu	$\sim$ 80 ms	8 transient cycles and 8 steady state cycles	< 1 kHz	Ideal trace calculated
[96]	I	L	Circuit with L parallel to CR	1.5 pu	$\sim$ 1 ms	1 transient cycle and 1 steady state cycle	< 2 kHz	Freq sweeps
[93]	I	L	Circuit with multiple resonances	60 - 100 A (Base values not specified)	650 μs	8 transient cycles and 8 steady state cycles	< 2 kHz	Ideal trace calculated
[49]	I (x2)	LCL	Simple RL	$\sim$ 0.5 pu	2 pulses: 0.5 ms and 0.7 ms	1 transient cycle and 1 steady state cycle	120 Hz - 2 kHz	Ideal trace calculated
[98]	V	LCL	Simple RL	0.1 pu	1 or 2 ms	Not specified	150 Hz - 1.65 kHz	Known RL

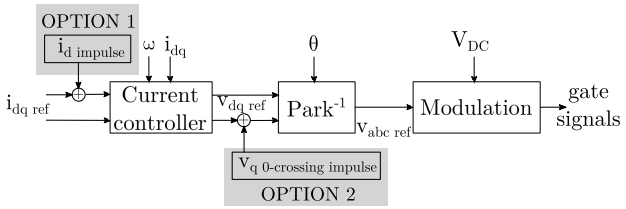

FIGURE 12. Typical locations of converter induced impulses. Pseudo random binary sequence injection location would be similar.

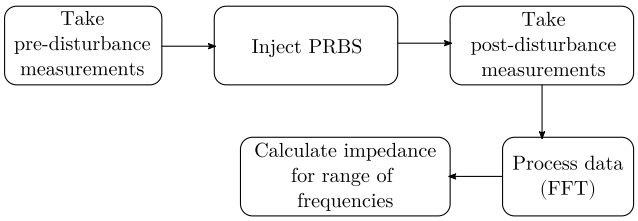

FIGURE 13. Flow chart for the PRBS technique.

to sinusoidal signals in order to decompose the signal into individual frequencies; whereas WT compares a given signal to wavelets [101]. There are multiple advantages to this: the WT is more suited to analysing a transient signal; and the WT is capable of identifying when a specific frequency appears in a signal and when it ends [102]. This is because the wavelet can be both compressed and expanded to accommodate for the various frequencies, but it can also be shifted, to undertake wavelet estimations at different time instances – unlike sine waves which are can be compressed and expanded but cannot be shifted (their shape does not change). With regards to the application of post-disturbance voltage and current analysis, as per [100], [103], the use of the WT has significantly reduced the number of periods required for pre- and post-disturbance analysis (from 8 periods to one period).

2) PSEUDO RANDOM BINARY SEQUENCE

The pseudo random binary sequence (PRBS) injection is a pre-determined sequence of wide-band excitation without the high total harmonic distortion (THD) of the impulse-response technique [21], [104], [105], with the flow chart presented in Fig. 13. These signals are in effect ones and zeros [106]. The length of the sequence, its magnitude and the switching frequency determines the achievable spectral resolution [107]. Compared to the impulse-response technique, this technique can work in much higher SNR conditions with significantly lower injection amplitude [82]. The spectral energy content of the injection can also be controlled in order to minimise interference with normal grid control and maximise the response of the desired frequencies [108]. Similarly to the impulse-response technique, FFT is applied to the measurements in order to estimate the spectral impedance [109], with the main advantage of improved immunity against the effect of nonlinear distortions.

V. QUASI-PASSIVE TECHNIQUES

Quasi-passive techniques combine an observer with an active technique. The observer is employed to identify *when* the network impedance may have changed. If it is determined that a change has occurred, the active technique is triggered. This a compromise between maximising quality of estimation and reducing the occurance of a disturbance injection: by tracking changes to the grid, a pre-determined criterion can initiate the active technique, introducing a disturbance on the system only when necessary [15], [98].

In [15], the trigger is a "quality threshold" (Γ). The quality threshold is the "voltage error", squared, divided by the current, averaged over a sampling window (22). It requires the latest grid impedance and grid voltage estimations as well as

TABLE 2. Classification of local impedance estimation techniques.

Technique	References	Target frequencies	Disturbance amplitude	Duration of disturbance	Are various SCR networks discussed?	Are various X/R ratios discussed?	Typical error	Comments	Data analysis technique
PMU (Adaptive)	[60]	ω_1	———	———	Yes	No, only $X_n >> R_n$	Inconclusive	Only relevant for transmission level	Adaptive
PMU (RLS)	[61]–[64]	ω_1	———	———	Yes	Yes	Low / Med	Stable estimations but not fast	RLS
PMU (Algebraic)	[24], [65]	ω_1	———	———	Yes	No, only $X_n/R_n = 0.2$	Inconclusive	Limited research undertaken	Algebraic
Observers	[19], [67]–[71], [110]	ω_1 to ω_{50}	———	———	Yes	Yes	Dependent on grid conditions	Dependent on grid event occurrence	FFT
Kalman Filter	[73], [74]	ω_1 only ω_1 to ω_{13}	———	———	Yes	No, only X/R ratios of < 1.2 tested	Low / Variable	Very complex	KF
Frequency sweeping	[1], [3], [5], [52], [75]–[77], [79], [80]	As required	~ 0.01 pu	$32 \times T_{fund}$ to ~ 1 min per harmonic	Yes	Yes	Low	Invasive and time consuming	FFT
Nonharmonic excitation (FFT)	[12]–[14], [83]–[85]	ω_1	0.05 to 0.077 pu	0.02 to 0.04 s	Yes	No, only X/R ratios of < 0.3 tested	Low / Med	Assumes linear impedance	FFT
Nonharmonic excitation (WT)	[11], [86]	ω_1	3 A (base unit not specified)	0.025 s	No	No	Low / Med	Assumes linear impedance	WT
Simultaneous frequency sweeping	[78]	As required	~ 0.02 pu per freq	0.01 to 1 s	No	No	Low	Invasive	FFT
P/Q reference variation	[15], [18], [25], [53], [87]–[91]	ω_1	Set-point step change 0.1% to 10%	~ 0.1 to 1 s	No	No, only X/R ratios of < 0.75 tested	Low / Med	Rate of estimation restricted by settling time	RLS or Algebraic
Hardware injected impulse-response	[2], [3], [7], [8], [81], [92]–[94]	ω_1 to 10 kHz	~ 1.5 to 5 pu	500 μs to 1.6 ms	Yes	Yes	Medium	High THD	FFT
Converter injected impulse-response (FFT)	[49], [96]–[99]	ω_1 to 2 kHz	0.1 to 1.5 pu	500 μs to 80 ms	Yes	Yes	Medium	High THD	FFT
Converter injected impulse-response (WT)	[100], [103]	ω_1 to 2 kHz	20 A (base units not specified)	1 ms	No	No	Inconclusive	High THD but lower processing time	WT
Pseudo random binary sequence injection	[21], [22], [82], [104], [105], [107]–[109], [111]	ω_1 to 3 kHz	0.1 to 0.2 pu	$5 \times T_{fund}$ to 1 s	Yes	Yes	Low / Med	Complex	FFT

voltage and current measurements. The window is k samples long. When the estimation values are correct, Γ should be close to zero.

$$\Gamma_k = \frac{1}{2k} \sum_{i=k-n}^{k+n} \frac{||V_i - I_{n\,i}\hat{Z}_{n\,i} - \hat{E}_i||^2}{|I_{n\,i}|} \tag{22}$$

Should a grid event affect the grid impedance, the estimation becomes outdated and Γ will increase. Once Γ goes past a pre-determined threshold, it triggers the estimation process [15].

Reference [98] proposes a Luenberger observer in order to trigger the active technique. The Luenberger observer is very similar to the Kalman Filter except that there is no change in ''correction'' gain and a linear state matrix is employed. The active technique is initiated when the difference between the estimated PCC voltage ($\hat{U} = f(I_n, \hat{E}, \hat{Z}_n)$) and the measured PCC voltage (U) exceeds a pre-determined magnitude ($\Delta U = U - \hat{U}$).

Quasi-passive techniques, however, introduce new delays due to the time required for the observer to detect an impedance change [15].

VI. COMPARISONS BETWEEN ESTIMATION TECHNIQUES

Table 2 presents a summary of the impedance estimation techniques found in the literature. The following items are compared in the table:

- Target frequencies: this column notes whether only the fundamental frequency (ω_1) is targeted, or whether the impedance estimation technique targets a range of frequencies per impedance estimation routine.
- Disturbance amplitude: Some techniques require large disturbances, and some require none at all – in which case the box is marked with a line.
- Disturbance duration: The duration of the disturbance per impedance estimation routine.
- Are various SCR networks discussed?: This column aims to identify if the various articles for each technique cover a range of network strengths. This aim of this is to identify whether some techniques are more popular to strong or weak networks.
- Are various X/R ratios discussed?: This column aims to identify if various impedance to resistance ratios are covered by the literature.
- Typical error: The estimations are sometimes compared to the name plate values, mathematical models of the experimental set-up or frequency sweep results, indicating how accurate the estimations are. Techniques that yield an error of <2% are considered to have low error. Between 2% and 5%, the error is medium. Any error larger than 5% is considered large.
- Comments: This column aims to highlight an important aspect of the technique which is not necessarily covered by the other columns.

- Data analysis techniques: Various analysis techniques are used such as FFT, WT, algebraic or RLS. This is important because not all microcontrollers may be able to handle some of the more intensive analysis techniques.

VII. RANKING OF TECHNIQUES BASED ON APPLICATION OBJECTIVES AND LIMITATIONS

All the above mentioned estimation techniques have advantages and disadvantages. The purpose of this section is to compare the techniques by explaining which would be more appropriate depending on the application objectives and limitations.

A. PRIORITISING ACCURACY

1) Frequency sweeping and honharmonic injection.
2) Simultaneous frequency sweeping.

The most accurate techniques are those ones which inject sinusoidal perturbations and utilise the steady state response for the estimation process. This includes both the frequency sweep technique and the nonharmonic injection technique. However, the former comes at the cost of a lengthy measurement period, and is therefore dependent on system stationarity for duration of the measurements. The latter is also dependent on stationarity (but to a lesser extent as disturbance injections are shorter), but it also assumes impedance linearity between the nonharmonic frequency and the fundamental frequency. Both techniques are also dependent on injecting an invasive, but low amplitude, disturbance. Worth considering, too, is the multi-sinusoidal injection described in [78].

B. PRIORITISING REDUCED NETWORK DISRUPTION

1) All PMU techniques, all observers and Kalman Filter.
2) Quasi-passive techniques (nonharmonic excitation).
3) P/Q variation.

With regards to minimising the disruption on the network, the best techniques are the passive techniques as no disturbance is injected. However, this comes at a cost of lower estimation accuracy and no control over disturbance interval (as only grid events introduce disturbances). However, if some noise is permitted, the use of quasi-passive techniques utilising nonharmonic excitation may be an acceptable compromise. Also, the P/Q variation techniques due to the low levels of injected noise (variations in outer loop references are much less disruptive than the injection of a sinusoidal or impulse disturbance).

C. MAXIMISING WIDE FREQUENCY-SPECTRUM IMPEDANCE ESTIMATION

1) Impulse-response and PRBS.
2) Frequency sweeping.

The best techniques for obtaining wide frequency range impedance estimations are the transient techniques, due to the short duration of the procedure. However, the frequency sweeping technique is also suitable, providing more accurate results but taking significantly more time.

D. PRIORITISING RAPIDITY OF ESTIMATION

1) Impulse-response and PRBS.
2) Nonharmonic excitation.
3) P/Q variation.

The best technique for a highly variable network is one which gives rapid estimation. As such, all transient techniques are adequate. If only the fundamental impedance is required then nonharmonic excitation or P/Q variation techniques are also acceptable with relatively short estimation times.

VIII. PRACTICAL USES FOR THE ESTIMATIONS

Estimation techniques may be suitable to a range of applications, and by discussing the techniques as a function of application may be useful to some readers. Note, however, that a large number of publications do not specify the intended use of the estimations, preferring to concentrate on the estimation process instead.

A. NETWORK CHARACTERISATION

The main priority in network characterisation is capture of wide frequency spectrum and temporal variations of the power network, in order to make power quality assessments and protection / filtering design decisions. This is covered in [8], [52], [75]–[77], [81], where the portability of the equipment is particularly important. Active techniques are required here, with the literature focused on frequency sweeps and impulse-response.

B. ANTI-ISLANDING DETECTION

Anti-islanding detection is mainly concerned with regular (periodic) estimates for Thévenin equivalent impedance magnitude, as this is sufficient for detection of unintentional islanding. Therefore, the main techniques utilised in the literature are the P/Q variation and the nonharmonic excitation techniques [12]–[15]. The most recent literature on this subject is [112], which focuses on applying an impedance estimation to detect islanding within 100 ms.

C. LC AND LCL FILTER RESONANCE AVOIDANCE

A number of papers use impedance estimation techniques to avoid resonating with the network, especially when passive damping has been avoided for efficiency reasons. The literature surrounding this is normally most concerned with the Thévenin equivalent impedance, resulting in the use of the P/Q variation technique [48] and the impulse-response technique proposed in [98]. Both of these techniques then use this information to tune the current controller, as the damping of filter resonances is primarily the function of the current controller [113]. The impulse-response technique is also used by [97] except the estimations are used to tune the

PLL and [49] which proposes ''impedance compensation'' in a modoified current controller.

D. CONTROLLER TUNING

With a variable grid impedance and the possibility of control-grid resonances, some authors have suggested using impedance estimation techniques specifically for current controller tuning purposes: [19], [70] use observers and [84] uses nonharmonic excitation. Some PRBS-type literature claim that their estimations can be used for adaptive control tuning [21], [82], but it is not specified what control aspect is being tuned. Reference [25] uses the P/Q variation technique to update the value of a virtual impedance within the PLL, intended to stabilise the controller in weak grids.

IX. FUTURE TRENDS

In the last decade, the literature on local impedance estimation has shifted fundamentally away from network characterisation (undertaken with specialised hardware) towards converter based online estimations for independent decision making processes. This shift happened at first with the objective of detecting islanding situations, and then with the aim of avoiding filter resonances and improved controller tuning. It is therefore reasonable to assume that online adaptation of converter control may become more widespread in the future, as network impedance variability continues to increase.

It is the authors' opinions that the literature on local estimation techniques is reaching maturity. It is expected that future literature will focus increasingly on the applications which utilise the estimations. These applications will likely use both wide frequency spectrum and Thévenin equivalent impedance estimation techniques, with the wide frequency spectrum impedance estimations employed for advanced resonance identification, and Thévenin equivalent impedance estimations for improving converter performance. This will become increasingly important as networks become more variable.

There are many options for research for future work, but the authors of this article would like to highlight the most promising areas.

1) There is limited research on the wavelet transform, which should be advantageous for both observer and impulse-response estimation techniques. The use of the wavelet transform would allow for improved extraction of transient signals over FFT and could significantly improve understanding of the network impedance.
2) The estimation of the impedance could be used to adapt the control and establish operational boundaries that improve stability, for example the maximum allowable power transfer limits of a converter.
3) Quasi-passive techniques are promising due to their accurate estimates and reduced perturbations. However, very few authors have explored the trigger implementations.
4) Few articles discuss the limitations of sensors and the computational capabilities of microcontrollers.

X. CONCLUSION

The motivations for local impedance estimations has evolved over the last decades. Initially, estimation techniques were driven by the need to understand the harmonic impedance through network characterisation studies. This has evolved to anti-islanding detection, LC and LCL filter resonance avoidance and online controller tuning.

This article has presented a review of impedance estimation techniques, produced a detailed classification and comprehensive description of the main impedance estimation techniques, and provided the reader with the tools required to compare the techniques and select the most appropriate technique for their application. Such considerations are, for example, the accuracy requirements of the estimation, the allowable noise that can be injected into the network, the required frequency range of the impedance estimation, and the time required for an estimation to be produced. Passive techniques, which inject no noise into the network, are less reliable in terms of estimation accuracy, frequency spectral range and time taken to produce an estimation. Active techniques provide much more control over the reoccurance of an estimation, the frequency spectral range and estimation accuracy at the cost of perturbation injection. Within active techniques, each method has its advantages and disadvantages.

As a final comment, it is worth highlighting the expected projection of impedance estimation techniques into the future. This will be driven, in large part, by the increased variability of network impedance. As a result, impedance estimations will probably be used to optimise controller tuning to ensure stability, adequate controller response and maximum power output.

DATA STATEMENT

There is no data supporting this review article other than the referenced material.

REFERENCES

[1] A. de Oliveira, J. C. de Oliveira, J. W. Resende, and M. S. Miskulin, ''Practical approaches for AC system harmonic impedance measurements,'' *IEEE Trans. Power Del.*, vol. 6, no. 4, pp. 1721–1726, Oct. 1991.
[2] M. Nagpal, W. Xu, and J. Sawada, ''Harmonic impedance measurement using three-phase transients,'' *IEEE Trans. Power Del.*, vol. 13, no. 1, pp. 272–277, Jan. 1998.
[3] A. Robert, T. Deflandre, E. Gunther, R. Bergeron, A. Emanuel, A. Ferrante, G. S. Finlay, R. Gretsch, A. Guarini, J. G. Iglesias, and D. Hartmann, ''Guide for assessing the network harmonic impedance,'' in *Proc. CIRED*, vol. 438, 1997, pp. 310-1–310-3.
[4] R. Redl, P. Tenti, and J. Daan van Wyk, ''Power electronics' polluting effects,'' *IEEE Spectr.*, vol. 34, no. 5, pp. 32–39, May 1997.
[5] M. Tsukamoto, S. Ogawa, Y. Natsuda, Y. Minowa, and S. Nishimura, ''Advanced technology to identify harmonics characteristics and results of measuring,'' in *Proc. 9th Int. Conf. Harmon. Qual. Power.*, vol. 1, 2000, pp. 341–346.
[6] Z. Staroszczyk, ''Accuracy problems in on-line one-phase distribution/load system identification task,'' in *Proc. IEEE Int. Symp. Ind. Electron.*, vol. 1, 1996, pp. 354–357.

[7] Z. Staroszczyk, "Problems in real-time wide band identification of power systems," in *Proc. Conf. IEEE Instrum. Meas. Technol. Conf.*, vol. 2, 1998, pp. 779–784.
[8] Z. Staroszczyk, "A method for real-time, wide-band identification of the source impedance in power systems," *IEEE Trans. Instrum. Meas.*, vol. 54, no. 1, pp. 377–385, Feb. 2005.
[9] M. Liserre, F. Blaabjerg, and R. Teodorescu, "Grid impedance detection via excitation of LCL-filter resonance," in *Proc. 14th IAS Annu. Meeting. Conf. Rec. Ind. Appl. Conf.*, vol. 2, 2005, pp. 910–916.
[10] M. Liserre, F. Blaabjerg, and R. Teodorescu, "Grid impedance estimation via excitation of *LCL*-filter resonance," *IEEE Trans. Ind. Appl.*, vol. 43, no. 5, pp. 1401–1407, 2007.
[11] S. C. Paiva, R. L. D. A. Ribeiro, D. K. Alves, F. B. Costa, and T. D. O. A. Rocha, "A wavelet-based hybrid islanding detection system applied for distributed generators interconnected to AC microgrids," *Int. J. Electr. Power Energy Syst.*, vol. 121, Oct. 2020, Art. no. 106032.
[12] A. V. Timbus, R. Teodorescu, F. Blaabjerg, and U. Borup, "Online grid measurement and ENS detection for PV inverter running on highly inductive grid," *IEEE Power Electron Lett.*, vol. 2, no. 3, pp. 77–82, Sep. 2004.
[13] L. Asiminoaei, R. Teodorescu, F. Blaabjerg, and U. Borup, "Implementation and test of an online embedded grid impedance estimation technique for PV inverters," *IEEE Trans. Ind. Electron.*, vol. 52, no. 4, pp. 1136–1144, Aug. 2005.
[14] L. Asiminoaei, R. Teodorescu, F. Blaabjerg, and U. Borup, "A digital controlled PV-inverter with grid impedance estimation for ENS detection," *IEEE Trans. Power Electron.*, vol. 20, no. 6, pp. 1480–1490, Nov. 2005.
[15] S. Cobreces, E. J. Bueno, D. Pizarro, F. J. Rodriguez, and F. Huerta, "Grid impedance monitoring system for distributed power generation electronic interfaces," *IEEE Trans. Instrum. Meas.*, vol. 58, no. 9, pp. 3112–3121, Sep. 2009.
[16] A. M. Massoud, K. H. Ahmed, S. J. Finney, and B. W. Williams, "Harmonic distortion-based island detection technique for inverter-based distributed generation," *IET Renew. Power Gener.*, vol. 3, no. 4, p. 493, 2009.
[17] *Utility-Interconnected Photovoltaic Inverters—Test Procedure of Islanding Prevention Measures BS EN 62116:2014*, BSI-Standards-Publication, 2014. [Online]. Available: https://shop.bsigroup.com/ProductDetail?pid=000000000030262010, doi: 10.1109/TIE.2005.851604.
[18] D. Sivadas and K. Vasudevan, "An active islanding detection strategy with zero nondetection zone for operation in single and multiple inverter mode using GPS synchronized pattern," *IEEE Trans. Ind. Electron.*, vol. 67, no. 7, pp. 5554–5564, Jul. 2020.
[19] A. Ghanem, M. Rashed, M. Sumner, M. A. Elsayes, and I. I. I. Mansy, "Grid impedance estimation for islanding detection and adaptive control of converters," *IET Power Electron.*, vol. 10, no. 11, pp. 1279–1288, Sep. 2017.
[20] N. Mohammed, M. Ciobotaru, and G. Town, "Online parametric estimation of grid impedance under unbalanced grid conditions," *Energies*, vol. 12, no. 24, p. 4752, Dec. 2019.
[21] R. Luhtala, T. Roinila, and T. Messo, "Implementation of real-time impedance-based stability assessment of grid-connected systems using MIMO-identification techniques," *IEEE Trans. Ind. Appl.*, vol. 54, no. 5, pp. 5054–5063, Sep. 2018.
[22] T. Roinila and T. Messo, "Online grid-impedance measurement using ternary-sequence injection," *IEEE Trans. Ind. Appl.*, vol. 54, no. 5, pp. 5097–5103, Sep. 2018.
[23] X. Zhang, D. Xia, Z. Fu, G. Wang, and D. Xu, "An improved feedforward control method considering PLL dynamics to improve weak grid stability of grid-connected inverters," *IEEE Trans. Ind. Appl.*, vol. 54, no. 5, pp. 5143–5151, Sep. 2018.
[24] B. Alinezhad and H. Kazemi Karegar, "On-line Thévenin impedance estimation based on PMU data and phase drift correction," *IEEE Trans. Smart Grid*, vol. 9, no. 2, pp. 1033–1042, Mar. 2018.
[25] H. Khazraj, F. Faria da Silva, and C. L. Bak, "An improved current controller to ensure the robust performance of grid-connected converters under weak grid conditions," in *Proc. IEEE 16th Int. Conf. Environ. Electr. Eng. (EEEIC)*, Jun. 2016, pp. 1–6.
[26] A. Egea-Alvarez, O. Gomis-Bellmunt, F. Hassan, and C. Barker, "Capability curves of a VSC-HVDC connected to a weak AC grid considering stability and power limits," in *Proc. 11th IET Int. Conf. AC DC Power Transmiss.*, 2015, p. 053.
[27] Y. Wang, B. Ren, and Q.-C. Zhong, "Robust power flow control of grid-connected inverters," *IEEE Trans. Ind. Electron.*, vol. 63, no. 11, pp. 6887–6897, Nov. 2016.
[28] K. Schaber, F. Steinke, P. Mühlich, and T. Hamacher, "Parametric study of variable renewable energy integration in europe: Advantages and costs of transmission grid extensions," *Energy Policy*, vol. 42, pp. 498–508, Mar. 2012.
[29] P. J. Baruah, N. Eyre, M. Qadrdan, M. Chaudry, S. Blainey, J. W. Hall, N. Jenkins, and M. Tran, "Energy system impacts from heat and transport electrification," *Proc. Inst. Civil Eng. Energy*, vol. 167, no. 3, pp. 139–151, Aug. 2014.
[30] S. Sumathi, L. A. Kumar, and P. Surekha, *Solar PV and Wind Energy Conversion Systems* (Green Energy and Technology). Cham, Switzerland: Springer, 2015.
[31] Seetharaman, K. Moorthy, N. Patwa, Saravanan, and Y. Gupta, "Breaking barriers in deployment of renewable energy," *Heliyon*, vol. 5, no. 1, Jan. 2019, Art. no. e01166.
[32] X. Koutiva, T. Vrionis, N. Vovos, and G. B. Giannakopoulos, "Optimal integration of an offshore wind farm to a weak AC grid," *IEEE Trans. Power Del.*, vol. 21, no. 2, pp. 987–994, Apr. 2006.
[33] M. Yu, A. J. Roscoe, A. Dyśko, C. D. Booth, R. Ierna, J. Zhu, and H. Urdal, "Instantaneous penetration level limits of non-synchronous devices in the British power system," *IET Renew. Power Gener.*, vol. 11, no. 8, pp. 1211–1217, Jun. 2017.
[34] H. Urdal, D. Rostom, A. Dahresobh, C. Ivanov, J. Zhu, and R. Ierna, "System strength considerations in a converter dominated power system," *IET Renew. Power Gener.*, vol. 9, no. 1, pp. 10–17, Jan. 2015.
[35] M. Cheah-Mane, L. Sainz, E. Prieto-Araujo, and O. Gomis-Bellmunt, "Impedance-based analysis of harmonic instabilities in HVDC-connected offshore wind power plants," *Int. J. Electr. Power Energy Syst.*, vol. 106, pp. 420–431, Mar. 2019.
[36] L. Zhang, "Modeling and control of VSC-HVDC links connected to weak AC systems," Ph.D. dissertation, KTH Royal Inst. Technol., Stockholm, Sweden, 2010.
[37] C. Guo, W. Liu, C. Zhao, and R. Iravani, "A frequency-based synchronization approach for the VSC-HVDC station connected to a weak AC grid," *IEEE Trans. Power Del.*, vol. 32, no. 3, pp. 1460–1470, Jun. 2017.
[38] O. Goksu, R. Teodorescu, C. L. Bak, F. Iov, and P. C. Kjaer, "Instability of wind turbine converters during current injection to low voltage grid faults and PLL frequency based stability solution," *IEEE Trans. Power Syst.*, vol. 29, no. 4, pp. 1683–1691, Jul. 2014.
[39] Q. Hu, L. Fu, F. Ma, and F. Ji, "Large signal synchronizing instability of PLL-based VSC connected to weak AC grid," *IEEE Trans. Power Syst.*, vol. 34, no. 4, pp. 3220–3229, Jul. 2019.
[40] M. F. M. Arani and Y. A.-R.-I. Mohamed, "Analysis and performance enhancement_newline of vector-controlled VSC in HVDC links connected to very weak grids," *IEEE Trans. Power Syst.*, vol. 32, no. 1, pp. 684–693, Jan. 2017.
[41] D. Yang, X. Ruan, and H. Wu, "Impedance shaping of the grid-connected inverter with LCL filter to improve its adaptability to the weak grid condition," *IEEE Trans. Power Electron.*, vol. 29, no. 11, pp. 5795–5805, Nov. 2014.
[42] J. Sun, Y. Wang, J. Gong, X. Zha, and S. Li, "Adaptability of weighted average current control to the weak grid considering the effect of grid-voltage feedforward," in *Proc. IEEE Appl. Power Electron. Conf. Expo. (APEC)*, Mar. 2017, pp. 3530–3535.
[43] W. Zhao and G. Chen, "Comparison of active and passive damping methods for application in high power active power filter with LCL-filter," in *Proc. Int. Conf. Sustain. Power Gener. Supply*, Apr. 2009, pp. 1–6.
[44] H. Komurcugil, S. Ozdemir, I. Sefa, N. Altin, and O. Kukrer, "Sliding-mode control for single-phase grid-connected LCL-filtered VSI with double-band hysteresis scheme," *IEEE Trans. Ind. Electron.*, vol. 63, no. 2, pp. 864–873, Feb. 2016.
[45] X. Chen, C. Y. Gong, H. Z. Wang, and L. Cheng, "Stability analysis of LCL-type grid-connected inverter in weak grid systems," in *Proc. Int. Conf. Renew. Energy Res. Appl. (ICRERA)*, Nov. 2012, pp. 1–6.
[46] R. Pena-Alzola, M. Liserre, F. Blaabjerg, M. Ordonez, and Y. Yang, "LCL-filter design for robust active damping in grid-connected converters," *IEEE Trans. Ind. Informat.*, vol. 10, no. 4, pp. 2192–2203, Nov. 2014.

[47] A. Adib, B. Mirafzal, X. Wang, and F. Blaabjerg, "On stability of voltage source inverters in weak grids," *IEEE Access*, vol. 6, pp. 4427–4439, 2018.

[48] D.-K. Choi and K.-B. Lee, "Stability improvement of distributed power generation systems with an LCL-filter using gain scheduling based on grid impedance estimations," *J. Power Electron.*, vol. 11, no. 4, pp. 599–605, Jul. 2011.

[49] X. Chen, Y. Zhang, S. Wang, J. Chen, and C. Gong, "Impedance-phased dynamic control method for grid-connected inverters in a weak grid," *IEEE Trans. Power Electron.*, vol. 32, no. 1, pp. 274–283, Jan. 2017.

[50] I. Sowa, J. L. Domínguez-García, and O. Gomis-Bellmunt, "Impedance-based analysis of harmonic resonances in HVDC connected offshore wind power plants," *Electric Power Syst. Res.*, vol. 166, pp. 61–72, Jan. 2019.

[51] R. Matica, V. Kirincic, S. Skok, and A. Marusic, "Transmission line impedance estimation based on PMU measurements," in *Proc. Eurocon*, Jul. 2013, pp. 1438–1444.

[52] J. P. Rhode, A. W. Kelley, and M. E. Baran, "Complete characterization of utilization-voltage power system impedance using wideband measurement," *IEEE Trans. Ind. Appl.*, vol. 33, no. 6, pp. 1472–1479, Nov. 1997.

[53] M. Ciobotaru, R. Teodorescu, P. Rodriguez, A. Timbus, and F. Blaabjerg, "Online grid impedance estimation for single-phase grid-connected systems using PQ variations," in *Proc. IEEE Power Electron. Spec. Conf.*, no. 1, Jun. 2007, pp. 2306–2312.

[54] *Measuring Relays and Protection Equipment—Part 118-1: Synchrophasor for Power Systems–Measurements*, document IEC/IEEE 60255-118-1, 2018.

[55] J. Ma, P. Zhang, H.-J. Fu, B. Bo, and Z.-Y. Dong, "Application of phasor measurement unit on locating disturbance source for low-frequency oscillation," *IEEE Trans. Smart Grid*, vol. 1, no. 3, pp. 340–346, Dec. 2010.

[56] Y. Guo, K. Li, Z. Yang, J. Deng, and D. M. Laverty, "A novel radial basis function neural network principal component analysis scheme for PMU-based wide-area power system monitoring," *Electr. Power Syst. Res.*, vol. 127, pp. 197–205, Oct. 2015.

[57] P. Dehghanian, B. Wang, and M. Tasdighi, *New Protection Schemes in Smarter Power Grids With Higher Penetration of Renewable Energy Systems*. Amsterdam, The Netherlands: Elsevier, 2019.

[58] H. Zhou, X. Zhao, D. Shi, H. Zhao, and C. Jing, "Calculating sequence impedances of transmission line using PMU measurements," in *Proc. IEEE Power Energy Soc. Gen. Meeting*, Jul. 2015, pp. 1–5.

[59] J. Yang, W. Li, T. Chen, W. Xu, and M. Wu, "Online estimation and application of power grid impedance matrices based on synchronised phasor measurements," *IET Gener., Transmiss. Distrib.*, vol. 4, no. 9, pp. 1052–1059, 2010.

[60] S. Corsi and G. N. Taranto, "A real-time voltage instability identification algorithm based on local phasor measurements," *IEEE Trans. Power Syst.*, vol. 23, no. 3, pp. 1271–1279, Aug. 2008.

[61] T. An, S. Zhou, J. Yu, W. Lu, and Y. Zhang, "Research on illed-conditioned equations in tracking thevenin equivalent parameters with local measurements," in *Proc. Int. Conf. Power Syst. Technol.*, no. 1, Oct. 2006, pp. 1–4.

[62] S.-J.-S. Tsai and K.-H. Wong, "On-line estimation of thevenin equivalent with varying system states," in *Proc. IEEE Power Energy Soc. Gen. Meeting Convers. Del. Elect. Energy 21st Century*, Jul. 2008, pp. 1–7.

[63] G. Fusco, A. Losi, and M. Russo, "Constrained least squares methods for parameter tracking of power system steady-state equivalent circuits," *IEEE Trans. Power Del.*, vol. 15, no. 3, pp. 1073–1080, Jul. 2000.

[64] J. Lavenius, L. Vanfretti, and G. N. Taranto, "Performance assessment of PMU-based estimation methods of thevenin equivalents for real-time voltage stability monitoring," in *Proc. IEEE 15th Int. Conf. Environ. Electr. Eng. (EEEIC)*, Jun. 2015, pp. 1977–1982.

[65] S. M. Abdelkader and D. J. Morrow, "Online tracking of Thévenin equivalent parameters using PMU measurements," *IEEE Trans. Power Syst.*, vol. 27, no. 2, pp. 975–983, May 2012.

[66] R. Isermann and M. Münchhof, *Identification of Dynamic Systems*. Berlin, Germany: Springer, 2011.

[67] D. Serfontein, J. Rens, G. Botha, and J. Desmet, "Continuous harmonic impedance assessment using online measurements," in *Proc. IEEE Int. Workshop Appl. Meas. Power Syst. (AMPS)*, Sep. 2015, pp. 1–6.

[68] D. Serfontein, J. Rens, G. Botha, and J. Desmet, "Continuous event-based harmonic impedance assessment using online measurements," *IEEE Trans. Instrum. Meas.*, vol. 65, no. 10, pp. 2214–2220, Oct. 2016.

[69] H. Gu, X. Guo, D. Wang, and W. Wu, "Real-time grid impedance estimation technique for grid-connected power converters," in *Proc. IEEE Int. Symp. Ind. Electron.*, May 2012, pp. 1621–1626.

[70] D. Perez-Estevez and J. Doval-Gandoy, "Grid impedance identification using the VSC switching ripple," in *Proc. IEEE Energy Convers. Congr. Expo. (ECCE)*, Sep. 2019, pp. 1506–1513.

[71] B. L. Eidson, D. L. Geiger, and M. Halpin, "Equivalent power system impedance estimation using voltage and current measurements," in *Proc. Clemson Univ. Power Syst. Conf.*, Mar. 2014, pp. 1–6.

[72] G. Welch and G. Bishop, "An introduction to the Kalman filter," Dept. Comput. Sci., Univ. North Carolina, Chapel Hill, NC, USA, Tech. Rep. TR95041, 2000. [Online]. Available: http://citeseerx.ist.psu.edu/viewdoc/download?doi=10.1.1.336.5576&rep=rep1&type=pdf

[73] N. Hoffmann and F. W. Fuchs, "Minimal invasive equivalent grid impedance estimation in Inductive–Resistive power networks using extended Kalman filter," *IEEE Trans. Power Electron.*, vol. 29, no. 2, pp. 631–641, Feb. 2014.

[74] J. Ye, Z. Zhang, A. Shen, J. Xu, and F. Wu, "Kalman filter based grid impedance estimating for harmonic order scheduling method of active power filter with output LCL filter," in *Proc. Int. Symp. Power Electron., Electr. Drives, Autom. Motion (SPEEDAM)*, Jun. 2016, pp. 359–364.

[75] L. Capponi, I. Fernandez, D. Roggo, A. Arrinda, I. Angulo, and D. De La Vega, "Comparison of measurement methods of grid impedance for narrow band-PLC up to 500 kHz," in *Proc. IEEE 9th Int. Workshop Appl. Meas. Power Syst. (AMPS)*, Sep. 2018, pp. 1–6.

[76] M. B. Harris, A. W. Kelley, J. P. Rhode, and M. E. Baran, "Instrumentation for measurement of line impedance," in *Proc. IEEE Appl. Power Electron. Conf. Expo. (ASPEC)*, Feb. 1994, pp. 887–893.

[77] D. Roggo, D. Furrer, and L. Merendaz, "On-line 2 to 150 kHz grid impedance meter," in *Proc. 22nd Int. Conf. Exhib. Electr. Distrib. (CIRED)*, 2013, p. 1417.

[78] A. Rygg and M. Molinas, "Real-time stability analysis of power electronic systems," in *Proc. IEEE 17th Workshop Control Modeling Power Electron. (COMPEL)*, Jun. 2016, pp. 1–7.

[79] Y. A. Familiant, J. Huang, K. A. Corzine, and M. Belkhayat, "New techniques for measuring impedance characteristics of three-phase AC power systems," *IEEE Trans. Power Electron.*, vol. 24, no. 7, pp. 1802–1810, Jul. 2009.

[80] G. Francis, R. Burgos, D. Boroyevich, F. Wang, and K. Karimi, "An algorithm and implementation system for measuring impedance in the D-Q domain," in *Proc. IEEE Energy Convers. Congr. Expo., Energy Convers. Innov. Clean Energy Future (ECCE)*, Sep. 2011, pp. 3221–3228.

[81] M. Sumner, B. Palethorpe, and D. Thomas, "Impedance measurement for improved power quality—Part 1: The measurement technique," *IEEE Trans. Power Del.*, vol. 19, no. 3, pp. 1442–1448, Jul. 2004.

[82] T. Roinila, M. Vilkko, and J. Sun, "Broadband methods for online grid impedance measurement," in *Proc. IEEE Energy Convers. Congr. Expo.*, Sep. 2013, pp. 3003–3010.

[83] R. Parthiban, T. Nivetha, and B. Umamaheswari, "Harmonic injection technique-based grid impedance estimation for an LCL-filtered grid connected inverter—An investigation," *Int. J. Power Electron.*, vol. 10, nos. 1–2, p. 155, 2019.

[84] M. Ciobotaru, R. Teodorescu, and F. Blaabjerg, "On-line grid impedance estimation based on harmonic injection for grid-connected PV inverter," in *Proc. IEEE Int. Symp. Ind. Electron.*, Jun. 2007, pp. 2437–2442.

[85] J. Kukkola, M. Routimo, and M. Hinkkanen, "Real-time grid impedance estimation using a converter," in *Proc. IEEE Energy Convers. Congr. Expo. (ECCE)*, Sep. 2019, pp. 6005–6012.

[86] D. K. Alves, R. L. A. Ribeiro, F. B. Costa, and T. O. A. Rocha, "Real-time wavelet-based grid impedance estimation method," *IEEE Trans. Ind. Electron.*, vol. 66, no. 10, pp. 8263–8265, Oct. 2019.

[87] A. V. Timbus, P. Rodriguez, R. Teodorescu, and M. Ciobotaru, "Line impedance estimation using active and reactive power variations," in *Proc. IEEE Power Electron. Spec. Conf.*, 2007, pp. 1273–1279.

[88] J. H. Suarez, H. M. C. Gomes, L. S. Santana, A. J. S. Filho, L. L. O. Carralero, and F. F. Costa, "An improved impedance estimation method based on power variations in grid-connected inverters," in *Proc. IEEE 15th Brazilian Power Electron. Conf. 5th IEEE Southern Power Electron. Conf. (COBEP/SPEC)*, Dec. 2019, pp. 1–6.

[89] S. Cobreces, F. Huerta, D. Pizarro, F. J. Rodrguez, and E. J. Bueno, "Three-phase power system parametric identification based on complex-space recursive least squares," in *Proc. IEEE Int. Symp. Intell. Signal Process.*, 2007, pp. 1–6.

[90] J. Fang, H. Deng, and S. M. Goetz, "Grid impedance estimation through grid-forming power converters," *IEEE Trans. Power Electron.*, vol. 36, no. 2, pp. 2094–2104, Feb. 2021.
[91] R. Fantino, C. A. Busada, and J. A. Solsona, "Grid impedance estimation by measuring only the current injected to the grid by a VSI with LCL filter," *IEEE Trans. Ind. Electron.*, early access, Feb. 20, 2020, doi: 10.1109/TIE.2020.2973910.
[92] L. S. Czarnecki and Z. Staroszczyk, "On-line measurement of equivalent parameters for harmonic frequencies of a power distribution system and load," *IEEE Trans. Instrum. Meas.*, vol. 45, no. 2, pp. 467–472, Apr. 1996.
[93] B. Palethorpe, M. Sumner, and D. W. P. Thomas, "System impedance measurement for use with active filter control," in *Proc. Power Electron. Variable Speed Drives*, no. 475, 2000, pp. 24–28.
[94] Z. Staroszczyk and A. Josko, "Real-time power system linear model identification: Instrumentation and algorithms," in *Proc. 17th IEEE Instrum. Meas. Technol. Conf.*, no. 1, May 2000, pp. 897–901.
[95] M. M. AlyanNezhadi, H. Hassanpour, and F. Zare, "Grid-impedance estimation in high-frequency range with a single signal injection using time–frequency distribution," *IET Sci., Meas. Technol.*, vol. 13, no. 7, pp. 1009–1018, Sep. 2019.
[96] M. Cespedes and J. Sun, "Online grid impedance identification for adaptive control of grid-connected inverters," in *Proc. IEEE Energy Convers. Congr. Expo. (ECCE)*, Sep. 2012, pp. 914–921.
[97] M. Cespedes and J. Sun, "Adaptive control of grid-connected inverters based on online grid impedance measurements," *IEEE Trans. Sustain. Energy*, vol. 5, no. 2, pp. 516–523, Apr. 2014.
[98] P. Garcia, M. Sumner, A. Navarro-Rodriguez, J. M. Guerrero, and J. Garcia, "Observer-based pulsed signal injection for grid impedance estimation in three-phase systems," *IEEE Trans. Ind. Electron.*, vol. 65, no. 10, pp. 7888–7899, Oct. 2018.
[99] M. Sumner, B. Palethorpe, D. W. P. Thomas, P. Zanchetta, and M. C. Di Piazza, "A technique for power supply harmonic impedance estimation using a controlled voltage disturbance," *IEEE Trans. Power Electron.*, vol. 17, no. 2, pp. 207–215, Mar. 2002.
[100] M. Sumner, D. W. P. Thomas, and P. Zanchetta, "Power system impedance estimation for improved active filter control, using continuous wavelet transforms," in *Proc. PES/TD*, 2006, pp. 653–658.
[101] K. G. Firouzjah, A. Sheikholeslami, and M. Khaleghi, "A new harmonic detection method for shunt active filter based on wavelet transform," *J. Appl. Sci.*, vol. 4, no. 11, pp. 1561–1568, 2008.
[102] M. Sifuzzaman, M. R. Islam, and M. Z. Ali, "Application of wavelet transform and its advantages compared to Fourier transform," *J. Phys. Sci.*, vol. 13, pp. 121–134, 2009. [Online]. Available: http://inet.vidyasagar.ac.in:8080/jspui/handle/123456789/779
[103] M. Sumner, A. Abusorrah, D. Thomas, and P. Zanchetta, "Real time parameter estimation for power quality control and intelligent protection of grid-connected power electronic converters," *IEEE Trans. Smart Grid*, vol. 5, no. 4, pp. 1602–1607, Jul. 2014.
[104] N. Mohammed, M. Ciobotaru, and G. Town, "Performance evaluation of wideband binary identification of grid impedance using grid-connected inverters," in *Proc. 21st Eur. Conf. Power Electron. Appl. (EPE ECCE Europe)*, Sep. 2019, pp. P.1–P.10
[105] A. Riccobono, E. Liegmann, A. Monti, F. Castelli Dezza, J. Siegers, and E. Santi, "Online wideband identification of three-phase AC power grid impedances using an existing grid-tied power electronic inverter," in *Proc. IEEE 17th Workshop Control Modeling Power Electron. (COMPEL)*, Jun. 2016, pp. 1–8.
[106] S. Neshvad, S. Chatzinotas, and J. Sachau, "Wideband identification of power network parameters using pseudo-random binary sequences on power inverters," *IEEE Trans. Smart Grid*, vol. 6, no. 5, pp. 2293–2301, Sep. 2015.
[107] D. Martin, I. Nam, J. Siegers, and E. Santi, "Wide bandwidth three-phase impedance identification using existing power electronics inverter," in *Proc. 28th Annu. IEEE Appl. Power Electron. Conf. Expo. (APEC)*, Mar. 2013, pp. 334–341.
[108] T. Roinila, M. Vilkko, and J. Sun, "Online grid impedance measurement using discrete-interval binary sequence injection," *IEEE J. Emerg. Sel. Topics Power Electron.*, vol. 2, no. 4, pp. 985–993, Dec. 2014.
[109] T. Roinila, T. Messo, and E. Santi, "MIMO-identification techniques for rapid impedance-based stability assessment of three-phase systems in DQ domain," *IEEE Trans. Power Electron.*, vol. 33, no. 5, pp. 4015–4022, May 2018.
[110] M. Esparza, J. Segundo, C. Gurrola-Corral, N. Visairo-Cruz, E. Barcenas, and E. Barocio, "Parameter estimation of a grid-connected VSC using the extended harmonic domain," *IEEE Trans. Ind. Electron.*, vol. 66, no. 8, pp. 6044–6054, Aug. 2019.
[111] D. Martin, E. Santi, and A. Barkley, "Wide bandwidth system identification of AC system impedances by applying pertubations to an existing converter," in *Proc. IEEE Energy Convers. Congr. Expo.*, Sep. 2011, pp. 2549–2556.
[112] M. Llonch-Masachs, D. Heredero-Peris, C. Chillón-Antón, D. Montesinos-Miracle, and R. Villafáfila-Robles, "Impedance measurement and detection frequency bandwidth, a valid island detection proposal for voltage controlled inverters," *Appl. Sci.*, vol. 9, no. 6, p. 1146, Mar. 2019.
[113] E. Twining and D. G. Holmes, "Grid current regulation of a three-phase voltage source inverter with an LCL input filter," *IEEE Trans. Power Electron.*, vol. 18, no. 3, pp. 888–895, May 2003.

MATHIEU KERVYN DE MEERENDRE (Student Member, IEEE) received the M.Eng. degree in mechanical engineering from the University of Bath, in 2014.

He has worked as a Project Engineer in both the aerospace and subsea engineering industries. In 2017, he joined Strathclyde with the Wind and Marine Energy Systems Centre of Doctoral Training (CDT). His research is focused on weak grid integration of renewable energy systems, with a focus on control, impedance estimation, low inertia networks, and microgrids.

EDUARDO PRIETO-ARAUJO (Member, IEEE) received the degree in industrial engineering from the School of Industrial Engineering of Barcelona (ETSEIB), Technical University of Catalonia (UPC), Barcelona, Spain, in 2011, and the Ph.D. degree in electrical engineering from UPC, in 2016. He joined CITCEA-UPC Research Group in 2010, and is currently a Serra Hunter Lecturer with the Electrical Engineering Department, UPC. His main interests are renewable generation systems, control of power converters for HVDC applications, interaction analysis between converters, and power electronics dominated power systems.

KHALED H. AHMED (Senior Member, IEEE) received the B.Sc. (Hons.) and M.Sc. degrees from Alexandria University, Egypt, in 2002 and 2004, respectively, and the Ph.D. degree in power electronics applications from the University of Strathclyde, U.K., in 2008. He has been appointed as a Professor at Alexandria University, Egypt, since 2019. He is currently a Reader in Power Electronics with the University of Strathclyde. He has published more than 100 technical articles in refereed journals and conferences as well as a published textbook *High Voltage Direct Current Transmission: Converters, Systems and DC Grids*, a book chapter contribution, and a PCT patent PCT/GB2017/051364. His research interests are renewable energy integration, high power converters, offshore wind energy, DC/DC converters, HVDC, and smart grids. He is a Senior Member of the IEEE Power Electronics and Industrial Electronics societies.

ORIOL GOMIS-BELLMUNT (Senior Member, IEEE) received the degree in industrial engineering from the School of Industrial Engineering of Barcelona (ETSEIB), Technical University of Catalonia (UPC), Barcelona, Spain, in 2001, and the Ph.D. degree in electrical engineering from UPC, in 2007.

In 1999, he joined Engitrol S.L., where he worked as the Project Engineer in the automation and control industry. Since 2004, he has been with the Electrical Engineering Department, UPC, where he is currently a Professor and participates in the CITCEA-UPC Research Group. Since 2020, he has been an ICREA Academia Researcher. His research interests include the fields linked with electrical machines, power electronics, and renewable energy integration in power systems.

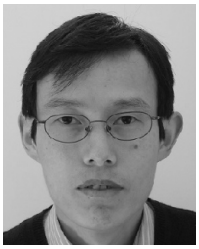

LIE XU (Senior Member, IEEE) received the B.Sc. degree in mechatronics from Zhejiang University, Hangzhou, China, in 1993, and the Ph.D. degree in electrical engineering from The University of Sheffield, Sheffield, U.K., in 2000.

He worked at Queen's University of Belfast and ALSTOM T&D, Stafford, U.K. He is currently a Professor with the Department of Electronic and Electrical Engineering, University of Strathclyde, Glasgow, U.K. His current research interests include power electronics, wind energy generation and grid integration, and application of power electronics to power systems. He is an Editor of the IEEE TRANSACTIONS ON POWER DELIVERY and the IEEE TRANSACTIONS ON ENERGY CONVERSION.

AGUSTÍ EGEA-ÀLVAREZ (Member, IEEE) received the B.Sc., M.Sc., and Ph.D. degrees from the Technical University of Catalonia, Barcelona, in 2008, 2010, and 2014, respectively.

In 2015, he was a Marie Curie Fellow with the China Electric Power Research Institute (CEPRI). In 2016, he joined Siemens Gamesa as a Converter Control Engineer working on grid forming controllers and alternative HVDC schemes for offshore wind farms. He is a member of the IET and has been involved in several CIGRE and ENTSOE working groups. He is currently a Strathclyde Chancellors Fellow (Lecturer) with the Electronic and Electrical Engineering Department and a member of the Power Electronics, Drives and Energy Conversion (PEDEC) Group since 2018. His current research interests include control and operation of high-voltage direct current systems, renewable generation systems, electrical machines, and power converter control.